Heliyon 9 (2023) e22435

Contents lists available at ScienceDirect

Heliyon

journal homepage: www.cell.com/heliyon

The effect of silica NPs incorporation on protective properties of oxide layers formed by PEO on $Mg_{97}Y_2Zn_1$ alloy with LPSO-phase

M.M. Krishtal [a], A.V. Katsman [a,b], A.V. Polunin [a,*], A.O. Cheretaeva [a]

[a] Togliatti State University, 445020, Tolyatti, Russian Federation
[b] Technion – Israel Institute of Technology, 32000 Haifa, Israel

ARTICLE INFO

Keywords:
Plasma electrolytic oxidation
Coating
Nanoparticles
Colliding interaction

ABSTRACT

The inherited chemical inhomogeneity in oxide layers obtained by plasma electrolytic oxidation (PEO) on the magnesium alloy $Mg_{97}Y_2Zn_1$ is associated to long-period stacking-ordered (LPSO) phase present in the treated alloy. This heterogeneity results in decrease of corrosion resistance and adhesion strength. The problem was solved by adding silica nanoparticles (NPs) into the electrolyte under PEO. According to the model developed, NPs which are harder than the oxide layer and being electrically charged, can be accelerated by an electric field and penetrate deep into the layer. The near-surface incorporation of NPs results in branching of the local breakdowns of vapor-gas bubbles that leads to an increase of the volumes of oxide layer and improvement of its properties.

1. Introduction

Outstanding progress was achieved recently in the engineering of magnesium alloys with a long-period stacking-ordered phase (LPSO-phase): the ultimate tensile strength and ductility of Mg-LPSO alloys were increased to the values ~600–800 MPa [1,2] and ~15–20 % and higher [2,3], respectively. However, the LPSO-phase led to the electric potential differences of the order of 60–250 mV between the α-Mg and the LPSO-phase [4,5]. This provokes the occurrence of microgalvanic corrosion in Mg-LPSO alloys and necessitates their surface protection, which can be solved by deposition of different coatings [6].

Plasma electrolytic oxidation (PEO) makes it possible to produce the wear- and corrosion-resistant oxide layers on the surface, coatings with high photocatalytic activity and polymer-ceramic coatings, and solves a wide range of tasks to ensure the required surface properties [7–16]. However, PEO of Mg-LPSO alloys has been used very rarely because of poor results under conventional regimes. Increase of PEO frequency up to >10 kHz reduced the porosity and corrosion current density about one order of magnitude or more compared to PEO at frequency 500 Hz or less on Mg-Gd-Y-Zr alloy [17]. The Ce-sealing after the PEO (sealing by CeO_2 release from the chemical solution) of Mg–Y–Zn alloy with LPSO-phase gave good corrosion protection; the lowest porosity (<2 %) and the highest anticorrosive properties of PEO layer were achieved [5].

It is well known that the use of various substances in the form of particles as a dispersion phase of the electrolyte under PEO is one of the most effective ways to improve the protective and functional properties of oxide coatings, as well as to increase the productivity and efficiency of the PEO technology [18–24]. The using of SiO_2, ZrO_2, TiN, Si_3N_4, TiO_2, TiC, MoS_2 particles, carbon nanotubes or halloysite nanotubes as additions to the electrolyte during PEO has led to significant improvement of wear- and corrosion resistance of

* Corresponding author.
E-mail address: anpol86@gmail.com (A.V. Polunin).

https://doi.org/10.1016/j.heliyon.2023.e22435
Received 24 August 2023; Received in revised form 28 October 2023; Accepted 13 November 2023
Available online 15 November 2023

formed oxide layers [21,25–30]. Silicon dioxide in a nanoscale form is one of the most proven substances as an additive to the electrolyte in the PEO of aluminum, magnesium and titanium alloys. It provides a significant increase in the wear resistance and corrosion resistance of oxide layers [21,25,31–35], is biocompatible [36–38] and, at the same time, relatively inexpensive. In recent years modifying PEO by adding various ceramic particles to the electrolyte has been widely studied for Mg-alloys such as Mg–Al–Zn, Mg–Mn–Ce and others [18,21,24,39,40]. However, as far as we know, the effects of using micro- or nanoparticles as dispersed phase of the electrolyte in PEO of Mg-LPSO alloys have not yet been investigated.

The behavior of nanoparticles (NPs) captured by vapor-gas bubbles (VGBs) prior the microarc discharge and their interaction with the surface of the oxide layer depend on various factors [28,41]. Most ceramic NPs are capable of adsorbing negative ions and electrons on their surface [42–44]. Getting into VGB the negatively charged nanoparticles accelerate by the applied electric field to very high velocities depending on their size: the smaller the particle the higher its final velocity [41]. This, as well as the ratio of the hardness of NPs and the oxide layer, leads to different scenarios of their interaction [28,41].

This work is aimed at revealing effects of adding silica NPs in the electrolyte on the PEO process of $Mg_{97}Y_2Zn_1$ alloy with LPSO-phase and elucidation of specific interaction mechanisms of silicon dioxide NPs and an oxide layer obtained during PEO.

2. Experimental procedures

Oxide layers were formed by PEO on flat specimens with sizes 20 × 60 × 6 mm^3 of $Mg_{97}Y_2Zn_1$ alloy with $Mg_{12}YZn$ LPSO-phase in alkaline-phosphate-fluoride-aluminate electrolyte at pulse frequency 1 kHz and duty cycle 50 % under constant current density 8 A/dm^2 within 10 min. PEO was provided without (specimens marked PEO (1 kHz)) and with addition of amorphous silica NPs (SiO_2 NPs, n-SiO_2) produced by Plasmotherm LLC (Moscow, Russia) with an average size of 100*nm* (size range – 56 ÷ 188*nm*) at a concentration 3 g/L (specimens PEO(1 kHz) + n-SiO_2). The concentration of NPs addition in the range of 2–3 g/L and specifically 3 g/L [39,41,45–48] has proven to be one of the most effective for achieving the best functional characteristics of oxide layers. The used silica NPs were characterized in detail in our previous work [41].

The aqueous solution of potassium hydroxide (KOH, 1 g/L), sodium phosphate disubstituted twelvehydrate ($Na_2HPO_4 \times 12H_2O$, 10 g/L), sodium phosphate (NaF, 10 g/L) and sodium aluminate ($NaAlO_2$, (10 g/L) was used as the base electrolyte. All reagents were of high chemical purity. The chemical composition of the alloy and preparatory procedures were described in Ref. [49].

The microstructure, chemical (elemental) and phase composition, thickness (T, μm), surface porosity (P_S, %) and effective porosity (P, %), hardness ($HV_{0.01}$, MPa), adhesion strength (specific critical load F_c, N/μm) and anticorrosive properties (corrosion potential E_{corr}, current density i_{corr}, polarization resistance R_p, impedance modulus $|Z|_{f\,=\,0.01Hz}$) were investigated by scanning electron microscopy (SEM), confocal laser scanning microscopy (CLSM), energy dispersive X-ray microanalysis (EDX), X-ray diffraction analysis (XRD), potentiodynamic polarization (PDP), electrochemical impedance spectroscopy (EIS) and instrumental methods using techniques described in Refs. [28,41,49].

3. Results and discussion

3.1. The evolution of forming voltages during PEO

The time evolution of anodic and cathodic forming voltages during the PEO process is shown on Fig. 1 for both electolytes used in the experiment. The electrolytes are marked as PEO and PEO+n-SiO_2 for electrolyte without and with silica NPs addition, respectively. In the first 100 s of PEO treatment, a rapid jump in the anodic voltage to 270 … 300 V was observed for both electrolytes. Then a slight increase in the anodic voltage was observed (up to values of 390 … 400 V at the end of the process), while the cathodic voltages were

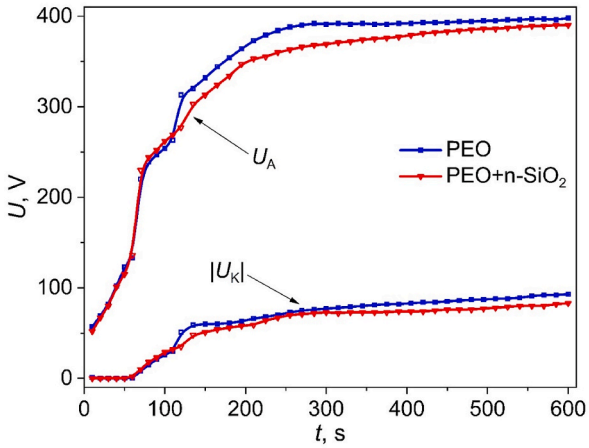

Fig. 1. Time dependencies of anodic (U_a) and cathodic (U_c) forming voltages under PEO treatment of $Mg_{97}Y_2Zn_1$ alloy in the case of base electrolyte (without n-SiO_2) and with addition of SiO_2 NPs.

significantly smaller than the anodic ones. In the first ~60 s, the cathode amplitude voltage was only ~1–2 V, then increased to 50–60 V, and then gradually rose to 80–90 V at the end of the PEO treatment. It can be assumed that the formation and compaction of the barrier layer at the magnesium alloy/electrolyte interface is the reason for the observed evolution of the anodic and cathodic voltages at the initial stage of the PEO process (Fig. 1). After ~100–120 s, the barrier layer probably acquires sufficient dielectric strength, which leads to a significant increase in the breakdown voltage, and then this characteristic changes slightly during the PEO process, and the corresponding increase in the forming voltages is relatively small.

It is important to note while the voltages behavior for both electrolytes during most of the PEO process is very similar, the forming voltages in the electrolyte with addition of silica NPs were clearly smaller than those in the base case (without addition of silica NPs to the electrolyte). The observed differences in the anodic voltages were about ~15–20 V after ~120 s and to ~5–10 V after ~450 s of the PEO treatment, while the difference in the values of cathodic voltages was ~5–10 V during most of the time processing. After an initial

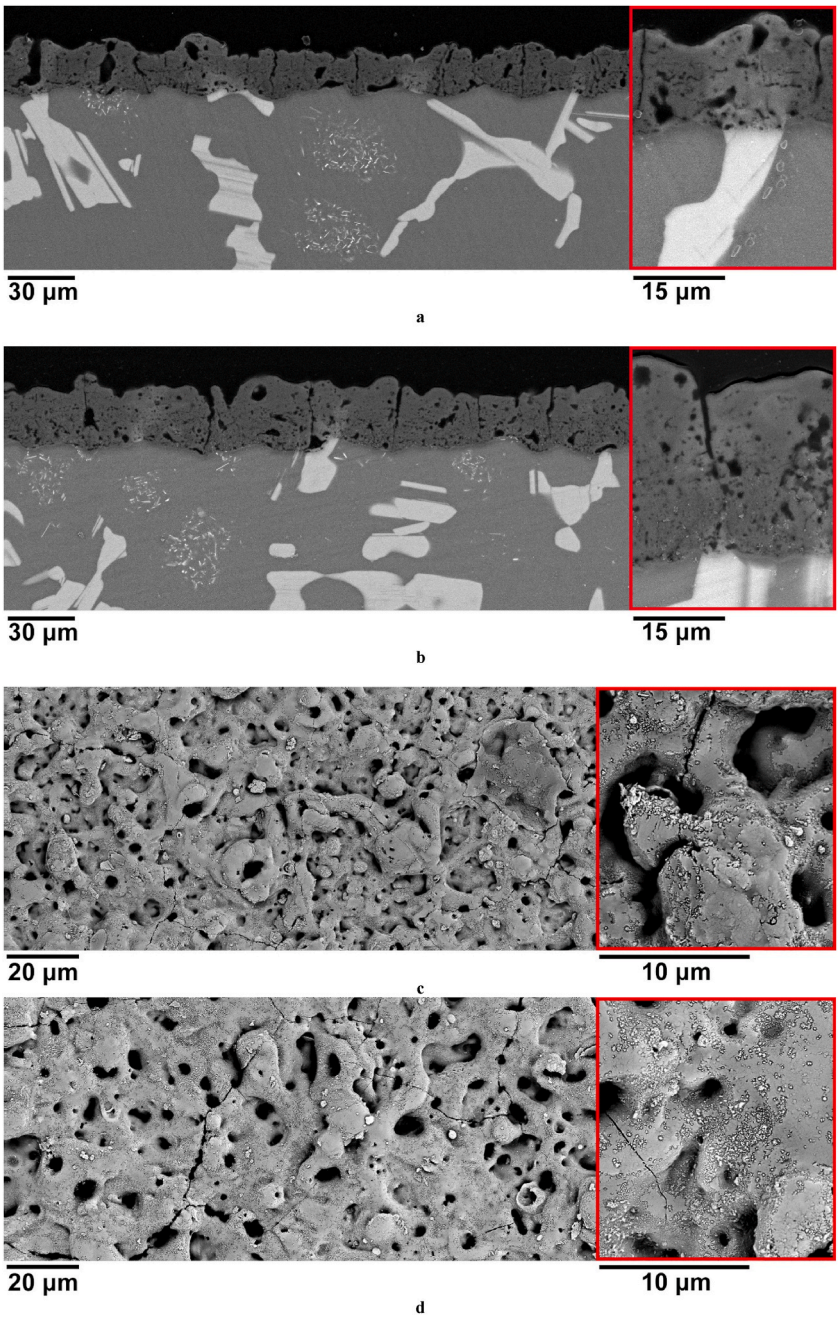

Fig. 2. Cross-section structure (a, b) and morphology of the surface (SEM, BSE) (c, d) of the layers obtained by PEO without (a, c) and with (b, d) n-SiO_2 addition.

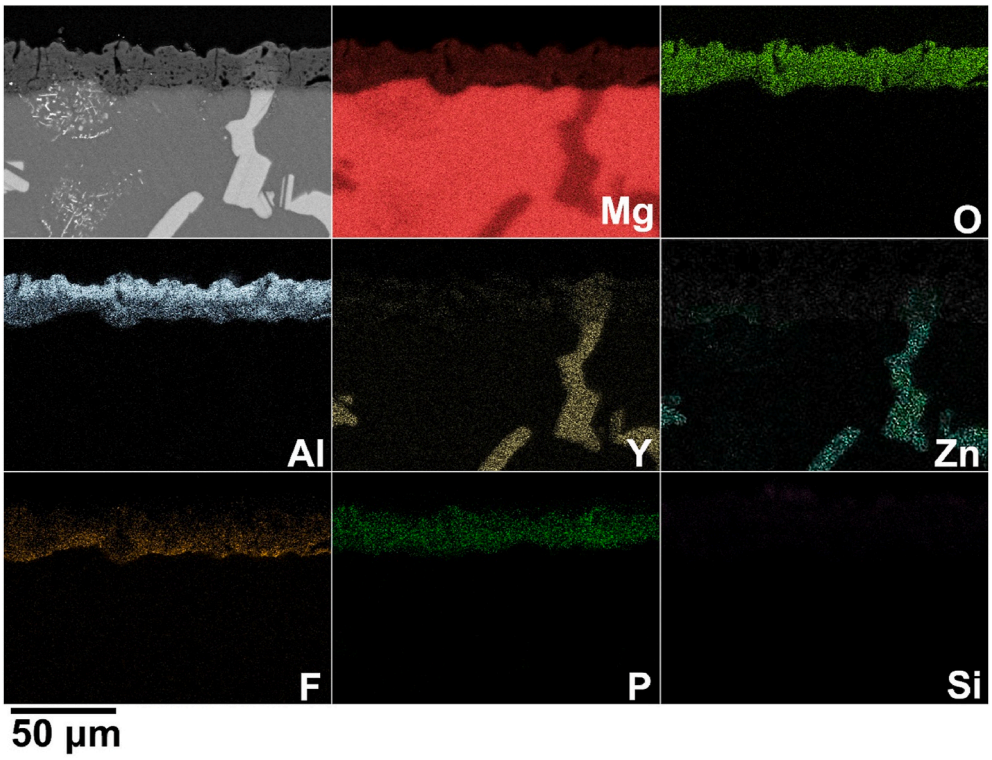

a

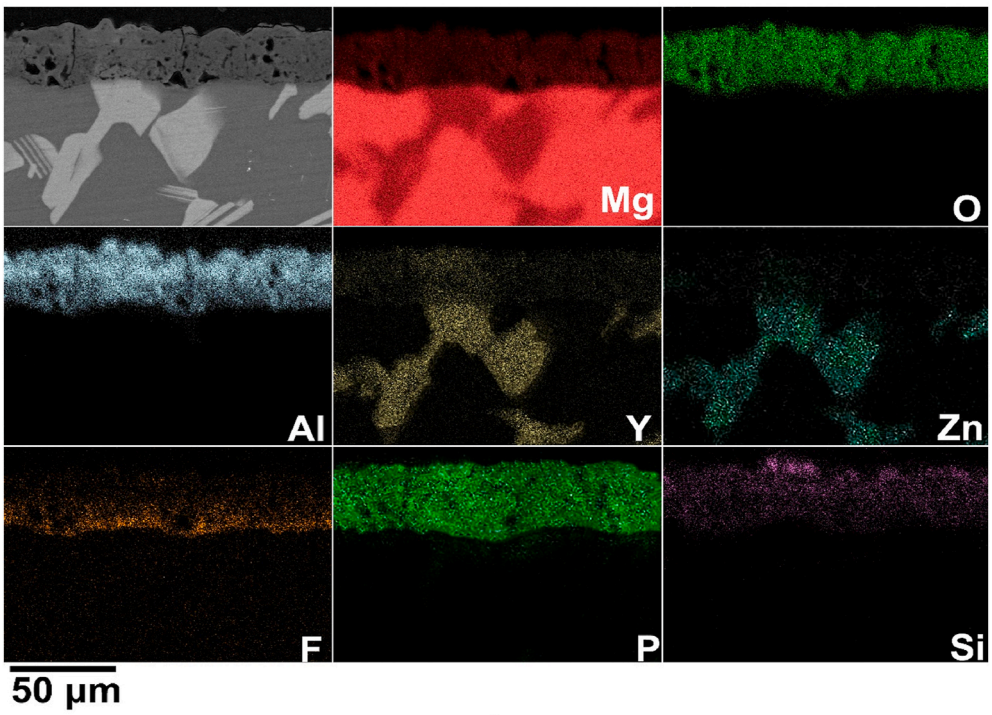

b

Fig. 3. The distribution maps of the main elements over the cross-sections (a, b) and on the surfaces (c, d) of the specimens obtained by PEO without (a, c) and with (b, d) n-SiO_2 addition.

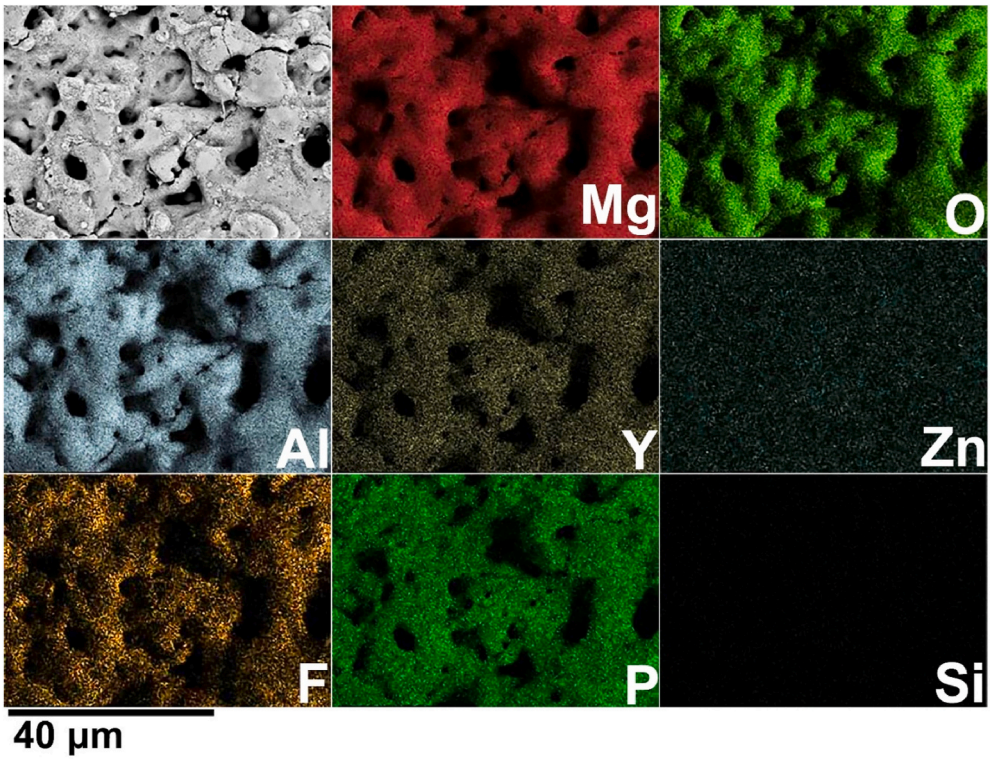

c

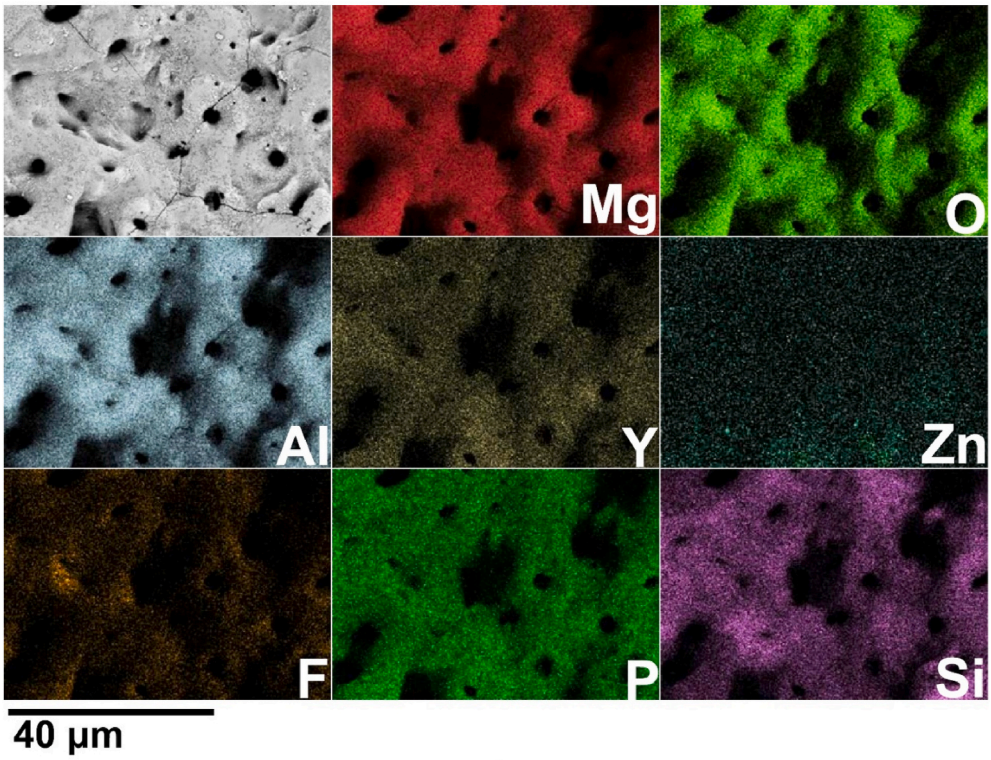

d

Fig. 3. (*continued*).

time of ~70–80 s of the PEO at voltages of about 240–250 V, visual sparking begins on the specimens in the bath, and then the brightness of microarc discharges and their number increase. Furthermore, the microarcs on the specimen in the electrolyte with the addition of SiO_2 NPs seemed to be brighter and sharper despite some turbidity of the electrolyte due to a suspension of silica NPs, which indicates their greater power compared to the sparks during PEO in the base electrolyte (without NPs). Finally the *n-SiO*$_2$ led to a decrease in the breakdown voltage during PEO in the anode and cathode half-periods at the end of the PEO process from 398 ± 2 V and 93 ± 1 V to 387 ± 2 V and 81 ± 1 V, respectively.

3.2. Structure, surface morphology and chemical composition of the oxide layers

It was found by phase contrast in SEM BSE mode and EDX, that the LPSO-phase is poorly oxidized that results in the hereditary chemical inhomogeneity (bright areas on the cross-section images – Fig. 2) of the formed layer, as well as in increase of porosity and discontinuities at the Mg-alloy/oxide layer interface (Fig. 2a and b). This phenomenon is confirmed by EDX-analysis showing that the bright areas are enriched by yttrium and zinc (Fig. 3a and b) transferred to the oxide layer from the LPSO-phase of the substrate. Furthermore, the presence of yttrium and zinc was detected on the surfaces of both specimens (Fig. 3c and d). A similar effect is known for PEO of Al–Si alloys as the inheritance of chemical inhomogeneity in the oxide layer from Si-particles of silumin [50].

The surface morphology of the obtained oxide layers has a strong unevenness, and contains cellular type zones, with numerous nanosized and microsized pan-cake elements, traces of hot gases, solidified bubbles, cracks and craters (Fig. 2c and d). Different micron and submicron objects resulting from micro breakdowns and subsequent thermal relaxation processes are seen in both cases.

Study of the oxide layer structure by SEM BSE and EDX methods revealed a nonuniform distribution of elements such as Zn and Y in the oxide layer cross-section which indicates LPSO-phase $Mg_{12}YZn$ (Fig. 3a and b), as well as fluorine F, which is detected predominantly in the inner zones of the obtained specimens (Fig. 3a and b). Other elements (Mg, Al, O and P, as well as Si in the case of addition of n-SiO_2 NPs in the electrolyte) are distributed quite uniformly over the cross-section structures (Fig. 3a and b) as well as on the surfaces of the specimens, without pronounced localizations near pores or on numerous plateaus of oxide layers (Fig. 3c and d).

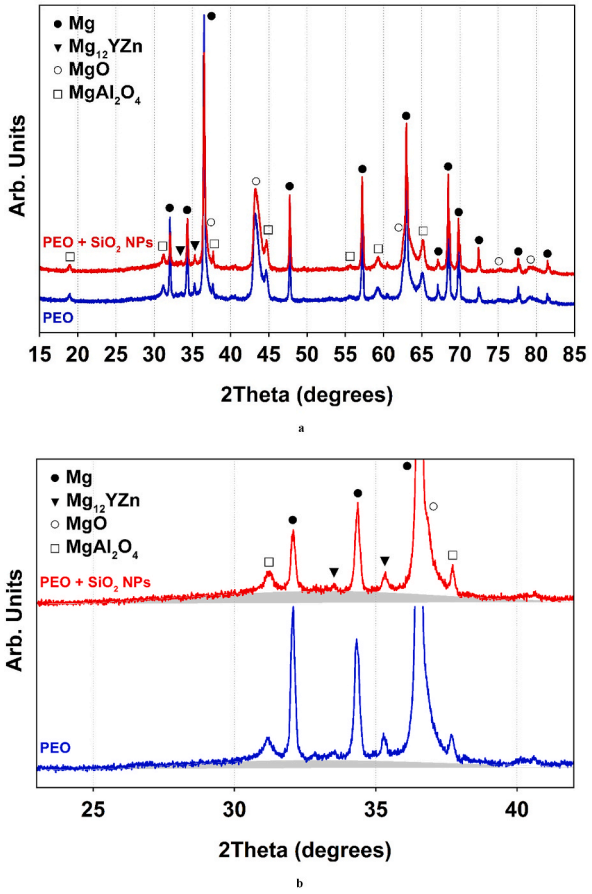

Fig. 4. XRD patterns of the $Mg_{97}Y_2Zn_1$ magnesium alloy samples with the oxide layers obtained by PEO in the base electrolyte (without silica NPs) and with n-SiO_2 additions to the electrolyte (a) and corresponding pattern's zones with broad peak (amorphous halos marked by grey) (b).

3.3. Coatings phase composition

The quantitative EDX analysis showed the presence of Si in the oxide layer (Figs. 2 and 3) in the amount of 2,18 ± 0,27 wt%, but no peaks of crystalline SiO_2 or products of chemical reactions of NPs with the oxide layer were detected by XRD (Fig. 4a). The both oxide layers consist of a mixture of magnesium oxide MgO (Hexagonal, *P*6$_3$/*mmc*) and magnesium aluminate $MgAl_2O_4$ (spinel, Cubic, Fd-3m) (Fig. 4a). It should be noted, that the broad peak (amorphous halo) in the range (25–40)° of the 2θ values (Fig. 4b) was observed which indicates the presence of a significant fraction of the amorphous phase being a part of the oxide layer.

A joint analysis of EDX and XRD results suggests that the silica NPs are incorporated in the coating in the initial chemical and structural state, without chemical reactions and/or recrystallization. Indeed, the incorporation of a silicon-containing substance into the oxide layer was established by EDX with a silicon content of ~2.2 wt % (which is equivalent to 4.7 wt% SiO_2). At the same time, XRD analysis did not show the presence of any reflections of silicon-containing crystalline phases, while showing an increase in the background signal (amorphous halo) and an increase in the fraction of the X-ray amorphous phase by ~4.4 wt% (Fig. 4, Table 1) that is near to addition of 4.7 % n-SiO_2. That is, the increase in the proportion of the amorphous phase practically coincides with the amount of SiO_2 (based on the conversion of Si detected by EDX to SiO_2). At the same time, the amount of magnesium oxide in the layer was at the same level of ~58.5 wt% for both cases (Table 1), which indicates the absence of reactions of magnesium oxide with SiO_2 NPs and is also confirmed by the absence of peaks of any of the magnesium silicate phases. Thus, according to detected XRD patterns and EDX data and calculated proportions of substances and phase compositions in the samples, a conclusion was made about the inert incorporation of SiO_2 nanoparticles into the layer. One can assume that some silica particles entered into reactions with the substances of the oxide layer and formed additional amorphous compounds in the composition of the amorphous phase. However, the proportion of such compounds is probably insignificant. In addition, it can be concluded, that phosphorus P and fluorine F are part of the X-ray amorphous phase, since no peaks of *P*-containing or *F*-containing phases were detected by XRD, but the presence of phosphorus and fluorine was detected by the EDX.

3.4. Protective properties of oxide layers

The addition of *n-SiO$_2$* to the electrolyte partially reduced the effect of hereditary chemical inhomogeneity (Fig. 2b), reduced the porosity *P* measured by PDP from ~0.19 % to ~0.07 %, surface porosity P_S measured by CLSM from ~1.5 % to ~1.2 % and roughness measured by CLSM from ~2.75 μm to ~2.60 μm, as well as provided an increase in the average coating thickness from ~22 μm to ~28 μm (Fig. 2, Tables 2 and 3).

The mechanical and corrosion tests showed that incorporation of n-SiO_2 in the oxide layer provided the increase in the adhesion strength and anticorrosion properties – the specific critical load F_c, polarization resistance R_p and impedance modulus $|Z|_{f\,=\,0.01Hz}$ increased by ~1.4, 6.3 and 2.5 times (Tables 2–4, Fig. 5), respectively, while corrosion current i_{corr} decreased by ~5.5 times (to ~4.7 nA/cm^2). The i_{corr} = 4,7 ± 0,3 nA/cm^2 (present research) is comparable to one of the best results achieved by PEO of the Mg-LPSO alloy followed by Ce-sealing post-treatment (2 nA/cm^2 [5]) and ~7 times less than the corrosion current obtained under ultra-high frequency PEO without NPs (~34 nA/cm^2 [17]).

The obtained Tafel plots (Fig. 5a), Nyquist plots (Fig. 5b), Bode plots (Fig. 5c) and phase angle plots (Fig. 5d) characterize the anticorrosive properties of the oxide layers. The results of processing the obtained dependencies are given in Table 3 (PDP) and Table 4 (EIS). It was found, that the presence of silica NPs in the electrolyte led to an increase of anticorrosive properties. It resulted in a decrease in the corrosion current i_{corr} by ~5.5 times (Table 3) and an increase in the anodic slope of the Tafel curve by ~ 1.6 times (Fig. 5a, Table 3), which together led to a high value of R_p according to Stern-Geary equation. The measured by EIS charge transfer resistance R_{in} through the barrier layer increased by ~2.5 times (Table 4). In addition, a decrease in the rate of anodic dissolution of magnesium and an increase in the passivity area by ~50–75 mV (some semblance of initial self-passivation) (while maintaining the value of catodic Tafel slope, β_c) can be observed (Fig. 5a, Table 3). This anodic passivation is probably responsible for the observed difference (more than 2.5 times) between R_p and $|Z|_{f\,=\,0.01Hz}$ (Tables 3 and 4). However, an additional investigation of this effect is needed and it will be a subject of our further research. In addition, the value of i_{corr} under maximum polarization voltage (+1.0 V vs OCP) in the case of PEO + n-SiO_2 specimen is about two order less against the base PEO specimen (Fig. 5a), which indicates its higher protective properties even in the case of high anodic polarization voltages. It can be assumed that the observed improvement of anticorrosive properties of coating obtained with addition of n-SiO_2 to the electrolyte can be partly due to incorporation of SiO_2 NPs into the barrier layer which leads to thickening and compaction of the barrier layer of the coating.

Table 1
Results of quantitative XRD analysis[a] of the obtained coatings.

Oxide Layer	Phase, wt%		
	MgO	$MgAl_2O_4$	Amorphous
PEO(1 kHz)	58.21	31.35	10.44
PEO(1 kHz) + n-SiO_2	58.66	26.54	14.8

[a] *The estimated error is less than 5 % (by factor wRp in the Jana 2006 software).*

Table 2
Measured characteristics of the formed oxide layers.

Oxide Layer	Thickness, T, μm	Roughness Sa, μm	Surface porosity, P_S, %	$HV_{0.01}$, MPa	F_c, N/μm
Bare alloy	–	–	–	67 ± 0,2 HB	–
PEO	22 ± 2.6	2.74 ± 0.26	1.48 ± 0.09	610 ± 120	1.1 ± 0.2
PEO + n-SiO_2	28 ± 3.5	2.58 ± 0.21	1.21 ± 0.12	600 ± 130	1.5 ± 0.2

Table 3
Corrosion properties of the bare $Mg_{97}Y_2Zn_1$ alloy and the alloy specimens with PEO layers obtained without and with silica NPs addition.

Sample	OCP, V	E_{corr}, V	i_{corr}, nA·cm^{-2}	β_c, V/dec	β_a, V/dec	R_p, kΩ·cm^2	P, %
Bare alloy	−1.58 ± 0.03	−1.47 ± 0.03	4600 ± 3641	0.10 ± 0.04	0.17 ± 0.09	7.6 ± 4.2	–
PEO	−1.53 ± 0.02	−1.54 ± 0.02	25.7 ± 11.5	0.18 ± 0.02	0.15 ± 0.06	(1.6 ± 0.8)[a]10^3	0.19 ± 0.08
PEO + n-SiO_2	−1.50 ± 0.06	−1.48 ± 0.01	4.7 ± 0.3	0.13 ± 0.04	0.24 ± 0.08	(9.8 ± 1.6)[a]10^3	0.07 ± 0.04

[a] *±2σ is provided as an error.*

Table 4
Calculated parameters of the equivalent electrical circuits for the $Mg_{97}Y_2Zn_1$ samples with various types of oxide layers.

Sample	R_{out}, kΩ·cm^2	CPE_{out}		R_{in}, MΩ·cm^2	CPE_{in}		$\|Z\|_{f\to 0.01Hz}$, MΩ·cm^2
		Q_{out}, $\Omega^{-1}\cdot cm^{-2}\cdot s^n$	n_{out}		Q_{in}, $\Omega^{-1}\cdot cm^{-2}\cdot s^n$	n_{in}	
Bare alloy	–	–	–	(1 ± 0.3)·10^{-3}	(1.6 ± 0.1)·10^{-5}	0.94 ± 0.01	(1.8 ± 0.2)·10^{-3}
PEO	10.5 ± 0.6	(3.0 ± 0.3)·10^{-7}	0.79 ± 0.01	1.27 ± 0.30	(1.5 ± 0.2)·10^{-7}	0.91 ± 0.03	1.34 ± 0.30
PEO + n-SiO_2	17.5 ± 2.3	(2.2 ± 0.1)·10^{-7}	0.80 ± 0.01	3.19 ± 1.10	(0.8 ± 0.1)·10^{-7}	0.95 ± 0.01	3.33 ± 0.13

±2σ is provided as an error.

3.5. The mechanism of the NP-oxide layer interaction during PEO

The following colliding interaction mechanism is suggested in order to explain an inert incorporation of NPs into the oxide layer during PEO. The negatively charged in the electrolyte NPs are captured by vapor-gas bubbles (VGBs), accelerated by an applied electric field to very high velocities and they hit forcibly the surface of the oxide layer prior the microarc discharge. The final velocity V achieved by the NP depends on the potential difference U in the way that the particle passes before colliding with the surface. For a spherical particle of mass m, diameter D and a charge q, the final velocity is the following:

$$V = \sqrt{\frac{2Uq}{m}} = \sqrt{\frac{12U\rho_q}{D\cdot\rho}} \tag{1}$$

where ρ_q is the surface charge density, ρ is the NP material density. If the particle is harder than the oxide coating, as in the case of silica NPs and magnesium oxide layer, it can penetrate deep into the layer almost without deformation. This leads to creation of a new nanochannel with a new surface in the layer. Kinetic energy of the particle is spent on creating this surface and heating the NP and the nanochannel walls which is associated with the friction of the particle against the new surface. In the case of a spherical particle the new surface will be approximately equal to the surface area of cylinder with a particle diameter D. The work to create this surface is

$$A_f = \gamma\pi DL \tag{2}$$

where γ is the effective surface energy taking into account a plastic deformation and heating of the layer material, L is the depth of the particle penetration into the oxide layer. Thus, the energy balance equation can be written as following:

$$\frac{mV^2}{2} = mC\Delta T + \gamma\pi DL \tag{3}$$

where C is the heat capacity of the NP substance, ΔT is the heat-up value of the particle. Considering $D \approx L$, one can estimate from eqs. (1)–(3) the value of heating. Using the typical known literature data for the surface charge density [51–53], $\rho_q = 0.1\,\frac{C}{m^2}$, the material properties of silicon dioxide: $C = 1\,\frac{kJ}{K\bullet kg}$, $\rho = 5\bullet 10^3\,\frac{kg}{m^3}$, $\gamma = 5\,\frac{J}{m^2}$, and using the difference of potentials across a VGB as $U = (100-200)V$, for the NP of diameter $D = 50$ nm, yields $\Delta T = (120-360)\,K$. This rather low heating explains inert incorporation of silica NPs in the oxide layer on Mg-alloy. On the other hand, the near-surface incorporation of NPs may lead to a local decrease of the breakdown voltage due to accumulation of positive surface charge during particle/surface friction. It therefore may lead to the appearance of additional microarcs and their branching (sparking) which were observed on the samples during PEO with the silica NPs addition.

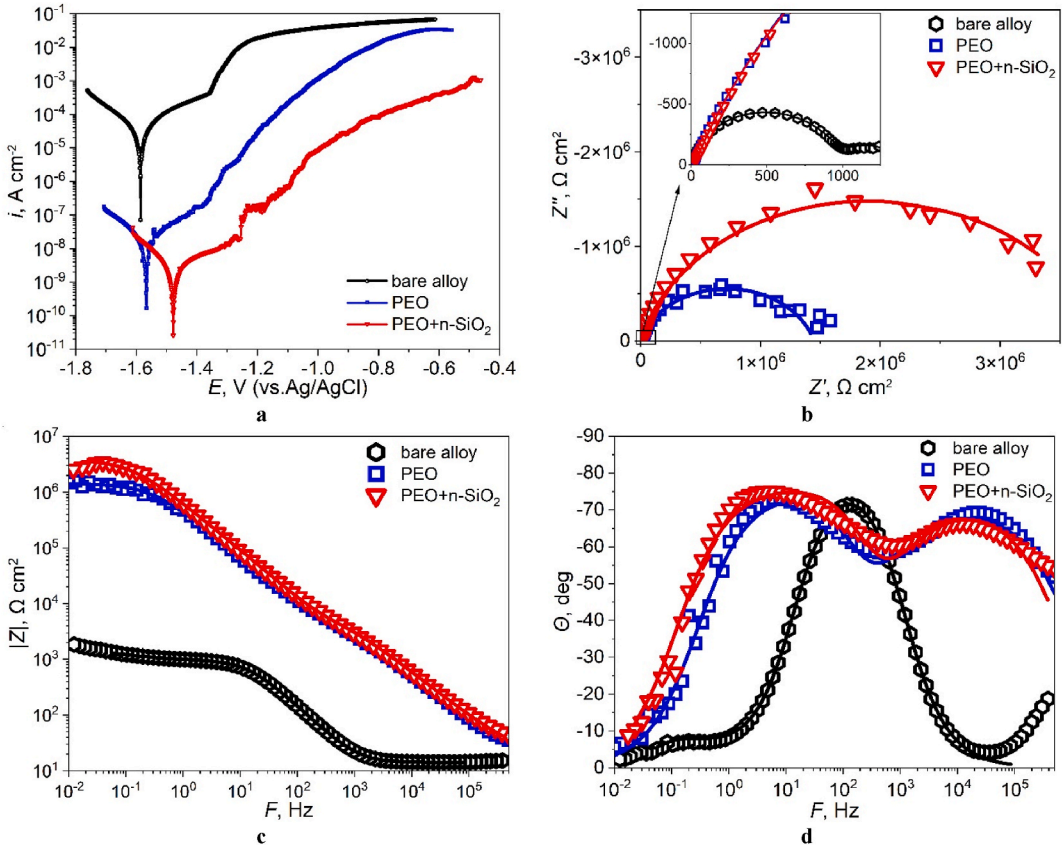

Fig. 5. Tafel plots (a), Nyquist plots (b), Bode plots (c) and phase angle plots (d) of the obtained specimens.

This, in turn, leads to an increase in the volume of the molted metal, and then the oxide layer volumes (increase of the coating thickness), similarly to the case of *n*- TiC using in PEO of Al–Si alloys [28].

4. Conclusion

The addition of silica NPs into the electrolyte led to a complex positive effect on the mechanical and anticorrosive properties of oxide layers obtained by PEO on Mg-LPSO alloy. The effect of hereditary chemical inhomogeneity caused by LPSO phase was partially reduced, the average coating thickness and adhesion strength were increased by ~28 % and ~36 %, respectively, the porosity was reduced by ~2.7 times and the corrosion current density by ~5.5 times. All these positive effects are associated with the change of number and power of microarc discharges. A certain decrease in the breakdown voltages caused by impact penetration of silica NPs into the oxide layer during their collisional interaction with the oxide layer during PEO treatment was observed and explained in the present work. The negatively charged and accelerated in electric field SiO_2 NPs collide with the forming coating and are embedded in the near-surface region almost without deformation being substantially harder than the oxide layer. It is suggested that this colliding interaction results in local accumulation of positive charges at the surface due to particle/surface friction. This, in turn, leads to appearance of additional local breakdowns and microarc branching responsible for increasing efficiency of the PEO process.

Data availability statement

Data associated with this study has not been deposited into a publicly available repository but it will be made available on request.

CRediT authorship contribution statement

M.M. Krishtal: Writing – review & editing, Validation, Supervision, Resources, Methodology, Funding acquisition, Formal analysis, Data curation, Conceptualization. **A.V. Katsman:** Writing – review & editing, Writing – original draft, Visualization, Validation, Methodology, Formal analysis, Data curation. **A.V. Polunin:** Writing – review & editing, Writing – original draft, Visualization, Validation, Resources, Project administration, Methodology, Investigation, Formal analysis, Data curation, Conceptualization. **A.O. Cheretaeva:** Writing – review & editing, Writing – original draft, Visualization, Validation, Methodology, Investigation, Formal

analysis, Data curation.

Declaration of competing interest

The authors declare that they have no known competing financial interests or personal relationships that could have appeared to influence the work reported in this paper.

Acknowledgement

The paper was supported by the Russian Science Foundation (project No. 21-19-00656, https://rscf.ru/project/21-19-00656/

References

[1] S. Ding, X. Cai, Z. Li, L. Xu, K. Wen, J. Song, H. Cui, H. Yu, T. Shen, Achieving ultra-strong Mg alloys via a novel hierarchical long-period stacking ordered architecture, J. Alloys Compd. 870 (2021), 159343, https://doi.org/10.1016/J.JALLCOM.2021.159343.
[2] S.M. Ramezani, A. Zarei-Hanzaki, H.R. Abedi, A. Salandari-Rabori, P. Minarik, Achievement of fine-grained bimodal microstructures and superior mechanical properties in a multi-axially forged GWZ magnesium alloy containing LPSO structures, J. Alloys Compd. 793 (2019) 134–145, https://doi.org/10.1016/J.JALLCOM.2019.04.158.
[3] K. Li, V.S.Y. Injeti, R.D.K. Misra, L.G. Meng, X.G. Zhang, The contribution of long-period stacking-ordered structure (LPSO) to high strength-high ductility combination and nanoscale deformation behavior of magnesium-rare earth alloy, Mater. Sci. Eng. 713 (2018) 112–117, https://doi.org/10.1016/J.MSEA.2017.12.056.
[4] C.Q. Li, D.K. Xu, Z.R. Zeng, B.J. Wang, L.Y. Sheng, X.B. Chen, E.H. Han, Effect of volume fraction of LPSO phases on corrosion and mechanical properties of Mg-Zn-Y alloys, Mater. Des. 121 (2017) 430–441, https://doi.org/10.1016/j.matdes.2017.02.078.
[5] M. Mohedano, P. Pérez, E. Matykina, B. Pillado, G. Garcés, R. Arrabal, PEO coating with Ce-sealing for corrosion protection of LPSO Mg–Y–Zn alloy, Surf. Coating. Technol. 383 (2020), 125253, https://doi.org/10.1016/J.SURFCOAT.2019.125253.
[6] V.S. Saji, Conversion Coatings for Magnesium and its Alloys, Springer International Publishing, 2022, https://doi.org/10.1007/978-3-030-89976-9.
[7] M. Kaseem, S. Fatimah, N. Nashrah, Y.G. Ko, Y. Gun Ko, Y.G. Ko, Y. Gun Ko, Y.G. Ko, Recent progress in surface modification of metals coated by plasma electrolytic oxidation: principle, structure, and performance, Prog. Mater. Sci. 117 (2021), 100735, https://doi.org/10.1016/J.PMATSCI.2020.100735.
[8] S. Sikdar, P.L.P.V. Menezes, R. Maccione, T. Jacob, P.L.P.V. Menezes, Plasma electrolytic oxidation (PEO) process—processing, properties, and applications, Nanomaterials 11 (2021) 1375, https://doi.org/10.3390/NANO11061375, 11 (2021) 1375.
[9] F. Simchen, M. Sieber, A. Kopp, T. Lampke, Introduction to plasma electrolytic oxidation-an overview of the process and applications, Coatings 10 (2020), https://doi.org/10.3390/COATINGS10070628.
[10] M. Karbasi, E. Nikoomanzari, R. Hosseini, H. Bahramian, R. Chaharmahali, S. Giannakis, M. Kaseem, A. Fattah-alhosseini, A review on plasma electrolytic oxidation coatings for organic pollutant degradation: how to prepare them and what to expect of them? J. Environ. Chem. Eng. 11 (2023), 110027 https://doi.org/10.1016/J.JECE.2023.110027.
[11] K.V. Nadaraia, S.N. Suchkov, I.M. Imshinetskiy, D.V. Mashtalyar, D.Y. Kosianov, E.A. Belov, S.L. Sinebryukhov, S.V. Gnedenkov, New superhydrophobic composite coatings on Mg-Mn-Ce magnesium alloy, J. Magnesium Alloys 11 (2023) 1721–1739, https://doi.org/10.1016/J.JMA.2023.03.006.
[12] D.V. Mashtalyar, K.V. Nadaraia, E.A. Belov, I.M. Imshinetskiy, S.L. Sinebrukhov, S.V. Gnedenkov, Features of composite layers created using an aqueous suspension of a fluoropolymer, Polym 14 (2022) 4667, https://doi.org/10.3390/POLYM14214667, 14 (2022) 4667.
[13] G.W. Lin, Y.H. Huang, W. Tseng, F.H. Lu, Production of N-doped anatase TiO2 on TiN-coated Ti substrates by plasma electrolytic oxidation for visible-light photocatalysts, Ceram. Int. 45 (2019) 22506–22512, https://doi.org/10.1016/J.CERAMINT.2019.07.275.
[14] S. Fatimah, F. Hazmatulhaq, Y. Sheng, T. Suhartono, J.M. Oh, N. Nashrah, J.-H. Kang, Y.G. Ko, Effect of ultrasonic frequency on structure and corrosion properties of coating formed on magnesium alloy via plasma electrolytic oxidation, Mater 16 (2023) 5424, https://doi.org/10.3390/MA16155424, 16 (2023) 5424.
[15] D.V. Mashtalyar, I.M. Imshinetskiy, K.V. Nadaraia, A.S. Gnedenkov, S.N. Suchkov, D.P. Opra, E.V. Pustovalov, A. Yu Ustinov, S.L. Sinebryukhov, S. V. Gnedenkov, Effect of TiO2 nanoparticles on the photocatalytic properties of PEO coatings on Mg alloy, J. Magnesium Alloys 11 (2023) 735–752, https://doi.org/10.1016/J.JMA.2022.10.021.
[16] N. Usmaniya, S. Radhakrishna Pillai, M. Palanivel, L. Edalacheruvu, P. Chennampalli, P. Vaithiyanathan, E. Parfenov, R.K. Lingamaneni, R. Nagumothu, Effect of polycaprolactone coating on the corrosion and biological characteristics of plasma electrolytic oxidised ZM21 magnesium alloy, Surf. Coating. Technol. 471 (2023), 129915, https://doi.org/10.1016/J.SURFCOAT.2023.129915.
[17] X. Liu, L. Liu, S. Dong, X.-B.B. Chen, J. Dong, Towards dense corrosion-resistant plasma electrolytic oxidation coating on Mg-Gd-Y-Zr alloy by using ultra-high frequency pulse current - ScienceDirect, Surf. Coating. Technol. 447 (2022), 128881, https://doi.org/10.1016/J.SURFCOAT.2022.128881.
[18] M. Molaei, K. Babaei, A. Fattah-alhosseini, Improving the wear resistance of plasma electrolytic oxidation (PEO) coatings applied on Mg and its alloys under the addition of nano- and micro-sized additives into the electrolytes: a review, J. Magnesium Alloys 9 (2021) 1164–1186, https://doi.org/10.1016/J.JMA.2020.11.016.
[19] A. Fattah-alhosseini, R. Chaharmahali, K. Babaei, Effect of particles addition to solution of plasma electrolytic oxidation (PEO) on the properties of PEO coatings formed on magnesium and its alloys: a review, J. Magnesium Alloys 8 (2020) 799–818, https://doi.org/10.1016/J.JMA.2020.05.001.
[20] L. An, Y. Ma, L. Sun, Z. Wang, S. Wang, Investigation of mutual effects among additives in electrolyte for plasma electrolytic oxidation on magnesium alloys, J. Magnesium Alloys 8 (2020) 523–536, https://doi.org/10.1016/j.jma.2019.09.003.
[21] X. Lu, C. Blawert, K.U. Kainer, T. Zhang, F. Wang, M.L. Zheludkevich, Influence of particle additions on corrosion and wear resistance of plasma electrolytic oxidation coatings on Mg alloy, Surf. Coating. Technol. 352 (2018) 1–14, https://doi.org/10.1016/J.SURFCOAT.2018.08.003.
[22] X. Lu, M. Mohedano, C. Blawert, E. Matykina, R. Arrabal, K.U. Kainer, M.L. Zheludkevich, Plasma electrolytic oxidation coatings with particle additions – a review, Surf. Coating. Technol. 307 (2016) 1165–1182, https://doi.org/10.1016/J.SURFCOAT.2016.08.055.
[23] M. Molaei, M. Nouri, K. Babaei, A. Fattah-Alhosseini, Improving surface features of PEO coatings on titanium and titanium alloys with zirconia particles: a review, Surface. Interfac. 22 (2021), 100888, https://doi.org/10.1016/J.SURFIN.2020.100888.
[24] J. Martin, P. Haraux, V. Ntomprougkidis, S. Migot, S. Bruyère, G. Henrion, Characterization of metal oxide micro/nanoparticles elaborated by plasma electrolytic oxidation of aluminium and zirconium alloys, Surf. Coating. Technol. 397 (2020), 125987, https://doi.org/10.1016/j.surfcoat.2020.125987.
[25] D. Mashtalyar, I. Imshinetsky, S. Sinebryukhov, S. Gnedenkov, Characterization of PEO-coatings on the MA8 magnesium alloy formed in electrolyte containing ZrO 2/SiO 2 nanoparticles, in: Mater. Today Proc., Elsevier Ltd, 2019, pp. 134–138, https://doi.org/10.1016/j.matpr.2018.12.120.
[26] I.M. Imshinetsky, S.V. Gnedenkov, S.L. Sinebryukhov, D.V. Mashtalyar, A.V. Samokhin, Y.V. Tsvetkov, Incorporation of composite zirconia-silica nanoparticles into PEO-coatings on magnesium alloys, Defect Diffusion Forum 386 (2018) 321–325, https://doi.org/10.4028/WWW.SCIENTIFIC.NET/DDF.386.321.
[27] A.V. Polunin, A.O. Cheretaeva, E.D. Borgardt, M.R. Shafeev, A.V. Katsman, M.M. Krishtal, Influence of nanoparticle additions to the electrolyte on the structure, composition and corrosion resistance of oxide layers formed by PEO on cast Mg alloy, J. Phys. Conf. Ser. 1713 (2020), 12036, https://doi.org/10.1088/1742-6596/1713/1/012036.

[28] A.V. Polunin, A.O. Cheretaeva, E.D. Borgardt, I.A. Rastegaev, M.M. Krishtal, A.V. Katsman, I.S. Yasnikov, Improvement of oxide layers formed by plasma electrolytic oxidation on cast AlSi alloy by incorporating TiC nanoparticles, Surf. Coating. Technol. 423 (2021), 127603, https://doi.org/10.1016/J.SURFCOAT.2021.127603.
[29] T. Zehra, M. Kaseem, S. Hossain, Y.G. Ko, Fabrication of a protective hybrid coating composed of tio2, moo2, and sio2 by plasma electrolytic oxidation of titanium, Met 11 (2021) 1182, https://doi.org/10.3390/met11081182, 11 (2021) 1182.
[30] I. Imshinetskiy, V. Kashepa, K. Nadaraia, D. Mashtalyar, S. Suchkov, P. Zadorozhny, A. Ustinov, S. Sinebryukhov, S. Gnedenkov, PEO coatings modified with halloysite nanotubes: composition, properties, and release performance, Int. J. Mol. Sci. 24 (2023) 305, https://doi.org/10.3390/IJMS24010305/S1.
[31] X. Lu, C. Blawert, Y. Huang, H. Ovri, M.L. Zheludkevich, K.U. Kainer, Plasma electrolytic oxidation coatings on Mg alloy with addition of SiO2 particles, Electrochim. Acta 187 (2016) 20–33, https://doi.org/10.1016/J.ELECTACTA.2015.11.033.
[32] Z. quan Huang, R. qiang Wang, H. Zhang, X. jie Shen, X. zhen Zhang, Y. He, C. Huang, D. jiu Shen, D. long Li, Effect of nanosized silicon dioxide additive on plasma electrolytic oxidation coatings fabricated on aluminium, Int. J. Electrochem. Sci. 15 (2020) 11191–11202, https://doi.org/10.20964/2020.11.24.
[33] X. Lu, Y. Chen, C. Blawert, Y. Li, T. Zhang, F. Wang, K.U. Kainer, M. Zheludkevich, Influence of SiO2 particles on the corrosion and wear resistance of plasma electrolytic oxidation-coated AM50 Mg alloy, Coatings 8 (2018) 306, https://doi.org/10.3390/COATINGS8090306, 8 (2018) 306.
[34] M.M. Krishtal, P.V. Ivashin, A.V. Polunin, E.D. Borgardt, The effect of dispersity of silicon dioxide nanoparticles added to electrolyte on the composition and properties of oxide layers formed by plasma electrolytic oxidation on magnesium 9995A, Mater. Lett. 241 (2019) 119–122, https://doi.org/10.1016/j.matlet.2019.01.080.
[35] M.M. Krishtal, P.V. Ivashin, A.V. Polunin, E.D. Borgardt, P.A. Glukhov, Effect of SiO2 nanoparticles and soluble silicate on the composition and properties of oxide layers formed by microarc oxidizing on magnesium Mg96, Met. Sci. Heat Treat. 61 (2019) 149–156, https://doi.org/10.1007/s11041-019-00391-5.
[36] J.P. Fernández-Hernán, A.J. López, B. Torres, E. Martínez-Campos, E. Matykina, J. Rams, Anticorrosion and cytocompatibility assessment of graphene-doped hybrid silica and plasma electrolytic oxidation coatings for biomedical applications, ACS Biomater. Sci. Eng. 7 (2021) 5861–5877, https://doi.org/10.1021/ACSBIOMATERIALS.1C00326/ASSET/IMAGES/LARGE/AB1C00326_0020. JPEG.
[37] X. Lu, C. Blawert, B.J.C. Luthringer, M.L. Zheludkevich, Controllable degradable plasma electrolytic oxidation coated Mg alloy for biomedical application, Front. Chem. Eng. 4 (2022), 748549, https://doi.org/10.3389/FCENG.2022.748549.
[38] F. Momeni, M.R. Rahimipour, S.M.M. Khoeia, A. Zamanian, A. Massoudi, A. Ghanbari, Optimization of the PEO process for in-situ synthesis of SiO2 and hydroxyapatite on Mg alloy and assessment of biodegradation and bioactivity, Surf. Coating. Technol. 468 (2023), 129774, https://doi.org/10.1016/J.SURFCOAT.2023.129774.
[39] D.V. Mashtalyar, S.V. Gnedenkov, S.L. Sinebryukhov, I.M. Imshinetskiy, A.V. Puz, Plasma electrolytic oxidation of the magnesium alloy MA8 in electrolytes containing TiN nanoparticles, J. Mater. Sci. Technol. 33 (2017) 461–468, https://doi.org/10.1016/j.jmst.2017.01.021.
[40] D.V. Mashtalyar, S.L. Sinebryukhov, I.M. Imshinetskiy, A.S. Gnedenkov, K.V. Nadaraia, A.Y. Ustinov, S.V. Gnedenkov, Hard wearproof PEO-coatings formed on Mg alloy using TiN nanoparticles, Appl. Surf. Sci. 503 (2020), 144062, https://doi.org/10.1016/j.apsusc.2019.144062.
[41] M.M. Krishtal, A.V. Katsman, A.V. Polunin, Effects of silica nanoparticles addition on formation of oxide layers on Al[sbnd]Si alloy by plasma electrolytic oxidation: the origin of stishovite under ambient conditions, Surf. Coating. Technol. 441 (2022), 128556, https://doi.org/10.1016/j.surfcoat.2022.128556.
[42] P. Rutberg, V. Kolikov, V. Snetov, A. Stogov, L. Noskin, S. Landa, A. Arutjunan, Pulsed Electric Discharges in Water and Oxide Nanoparticles, 16th IEEE Int. Pulsed Power Conf., 2007, 2007, pp. 1244–1247, https://doi.org/10.1109/PPPS.2007.4652412.
[43] Q. Liu, Z. Sun, J.C. Santamarina, Transport and adsorption of silica nanoparticles in carbonate reservoirs: a sand column study, Energy Fuel. 33 (2019) 4009–4016, https://doi.org/10.1021/ACS.ENERGYFUELS.9B00057/SUPPL_FILE/EF9B00057_SI_001.PDF.
[44] C.P. Romero, R.I. Jeldres, G.R. Quezada, F. Concha, P.G. Toledo, Zeta potential and viscosity of colloidal silica suspensions: effect of seawater salts, pH, flocculant, and shear rate, Colloids Surfaces A Physicochem. Eng. Asp. 538 (2018) 210–218, https://doi.org/10.1016/J.COLSURFA.2017.10.080.
[45] M.M. Krishtal, A.V. Polunin, P.V. Ivashin, E.D. Borgardt, I.S. Yasnikov, Changes in the phase composition of oxide layers produced by microarc oxidation on Al–Si and Mg alloys induced by additions of SiO2 nanoparticles to the electrolyte, Dokl. Phys. Chem. 469 (2016) 93–96, https://doi.org/10.1134/S0012501616070010.
[46] A. Apelfeld, B. Krit, V. Ludin, N. Morozova, B. Vladimirov, R.Z. Wu, The characterization of plasma electrolytic oxidation coatings on AZ41 magnesium alloy, Surf. Coating. Technol. 322 (2017) 127–133, https://doi.org/10.1016/J.SURFCOAT.2017.05.048.
[47] B.S. Lou, Y.Y. Lin, C.M. Tseng, Y.C. Lu, J.G. Duh, J.W. Lee, Plasma electrolytic oxidation coatings on AZ31 magnesium alloys with Si3N4 nanoparticle additives, Surf. Coating. Technol. 332 (2017) 358–367, https://doi.org/10.1016/j.surfcoat.2017.05.094.
[48] M. Ghafaripoor, K. Raeissi, M. Santamaria, A. Hakimizad, The corrosion and tribocorrosion resistance of PEO composite coatings containing α-Al2O3 particles on 7075 Al alloy, Surf. Coating. Technol. 349 (2018) 470–479, https://doi.org/10.1016/j.surfcoat.2018.06.027.
[49] A.O. Cheretaeva, P.A. Glukhov, M.R. Shafeev, A.G. Denisova, E.D. Borgardt, A.V. Polunin, A.V. Katsman, M.M. Krishtal, Improvement of protective oxide layers formed by high-frequency plasma electrolytic oxidation on Mg-RE alloy with LPSO-phase, Chim. Techno Acta. 10 (2023), 202310212, https://doi.org/10.15826/chimtech.2023.10.2.12.
[50] M.M. Krishtal, M.Y. Ryumkin, Inherited chemical inhomogeneity in oxide layers deposited by the method of microarc oxidizing on hypereutectic silumins, Met. Sci. Heat Treat. 49 (2007) 111–117, https://doi.org/10.1007/s11041-007-0021-x.
[51] B.O. Alan, M. Barisik, H.G. Ozcelik, Roughness effects on the surface charge properties of silica nanoparticles, J. Phys. Chem. C 124 (2020) 7274–7286, https://doi.org/10.1021/ACS.JPCC.0C00120/ASSET/IMAGES/MEDIUM/JP0C00120_0016. GIF.
[52] Y.R. Shi, M.P. Ye, L.C. Du, Y.X. Weng, Experimental determination of particle size-dependent surface charge density for silica nanospheres, J. Phys. Chem. C 122 (2018) 23764–23771, https://doi.org/10.1021/acs.jpcc.8b07566.
[53] M. Barisik, S. Atalay, A. Beskok, S. Qian, Size dependent surface charge properties of silica nanoparticles, J. Phys. Chem. C 118 (2014) 1836–1842, https://doi.org/10.1021/jp410536n.